Electronic Supplementary Material (ESI) for Inorganic Chemistry Frontiers.

Supporting Information

Mild construction phosphorus-based "integrated" electrode for efficient and durable seawater splitting at large current density

Jiajing Xia[a#], LuJia Zhang[a#], Yizhou Wang[b], Weiju Hao[a*]

[a] University of Shanghai for Science and Technology, Shanghai 200093, PR China.

[b] Hubei Key Laboratory of Energy Storage and Power Battery, School of Mathematics, Physics and Optoelectronic Engineering, Hubei University of Automotive Technology, Shiyan 442002, PR China.

[#] The authors are equal to this work.

E-mail: wjhao@usst.edu.cn

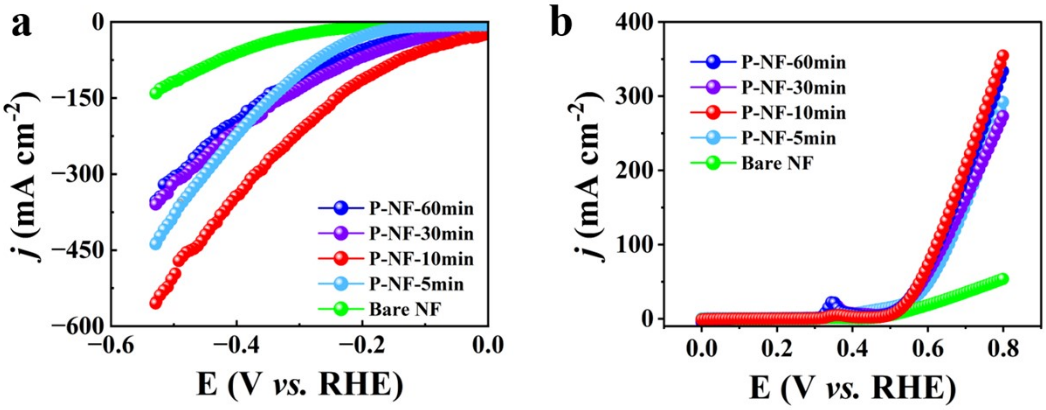

Figure S1 LSV curves of P-NF with different plating time (a) during HER process and (b) during OER process in 1.0 M KOH + 0.5 M NaCl.

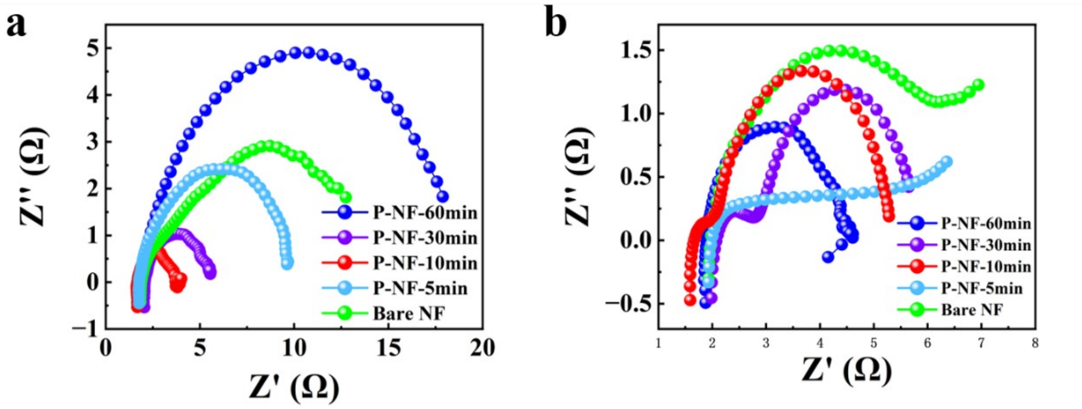

Figure S2 EIS curves of P-NF with different plating time (a) during HER process and (b) during OER process in 1.0 M KOH + 0.5 M NaCl.

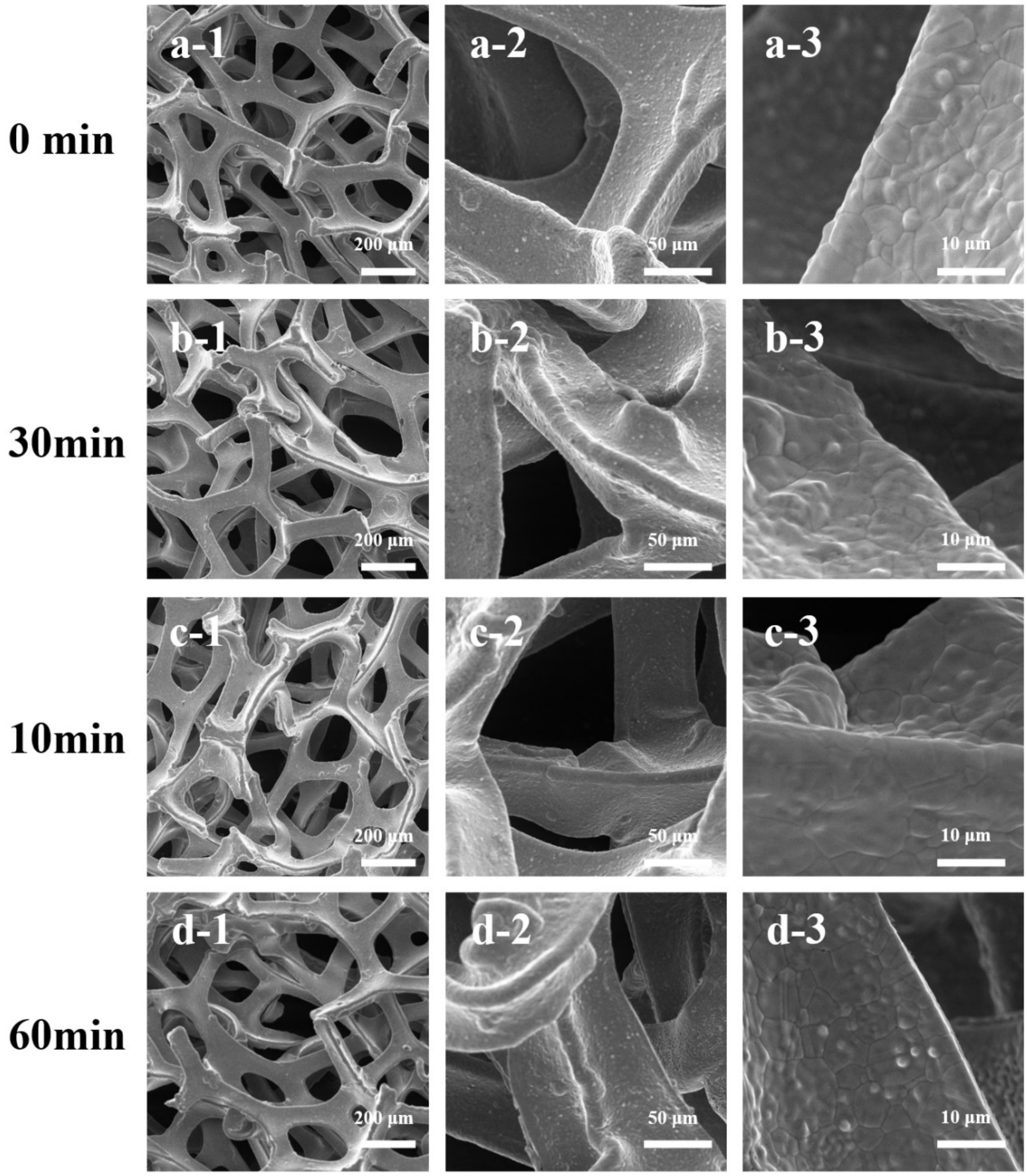

Figure S3 SEM images of P-NF with different reaction time (0, 30, 10 and 60 min).

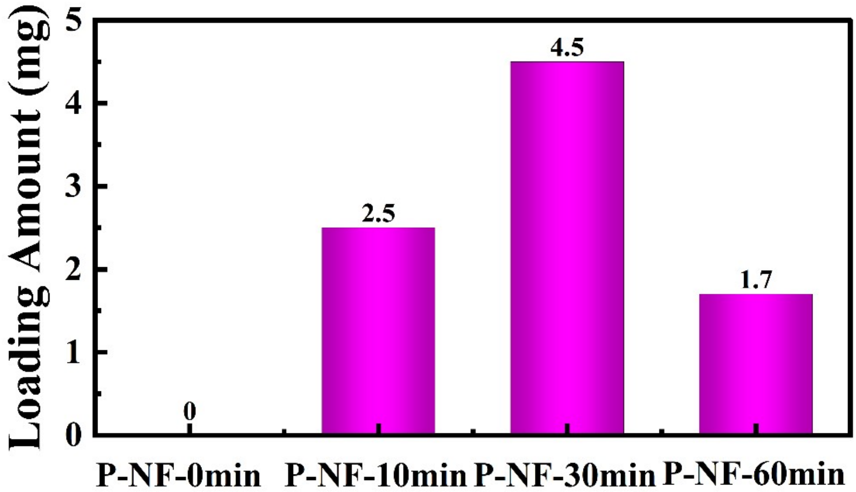

Figure S4 The loading amount of NaH_2PO_2 on NF substrate with different electroless plating time.

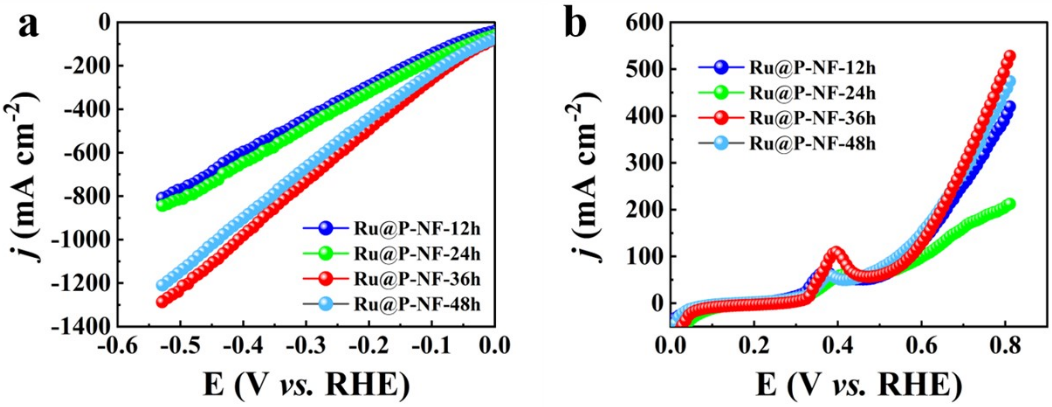

Figure S5 LSV curves of Ru@P-NF with different plating time (a) during HER process and (b) during OER process in 1.0 M KOH + 0.5 M NaCl.

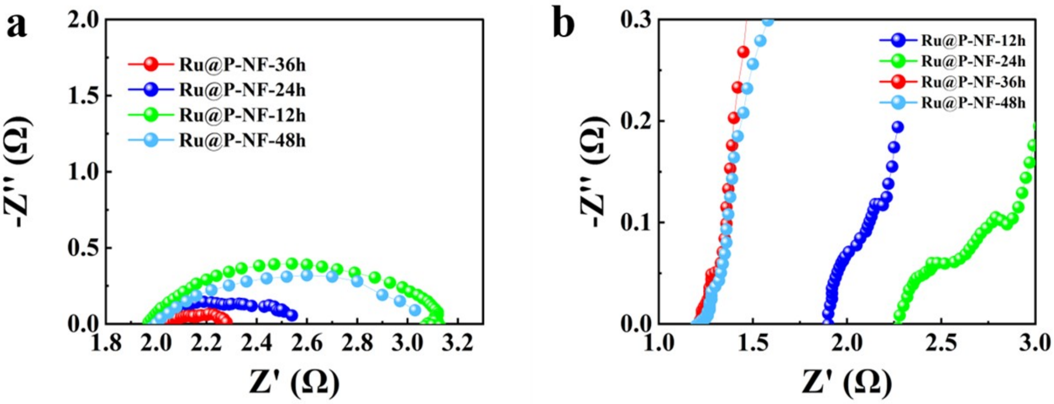

Figure S6 EIS curves of Ru@P-NF with different plating time (a) during HER process and (b) during OER process in 1.0 M KOH + 0.5 M NaCl.

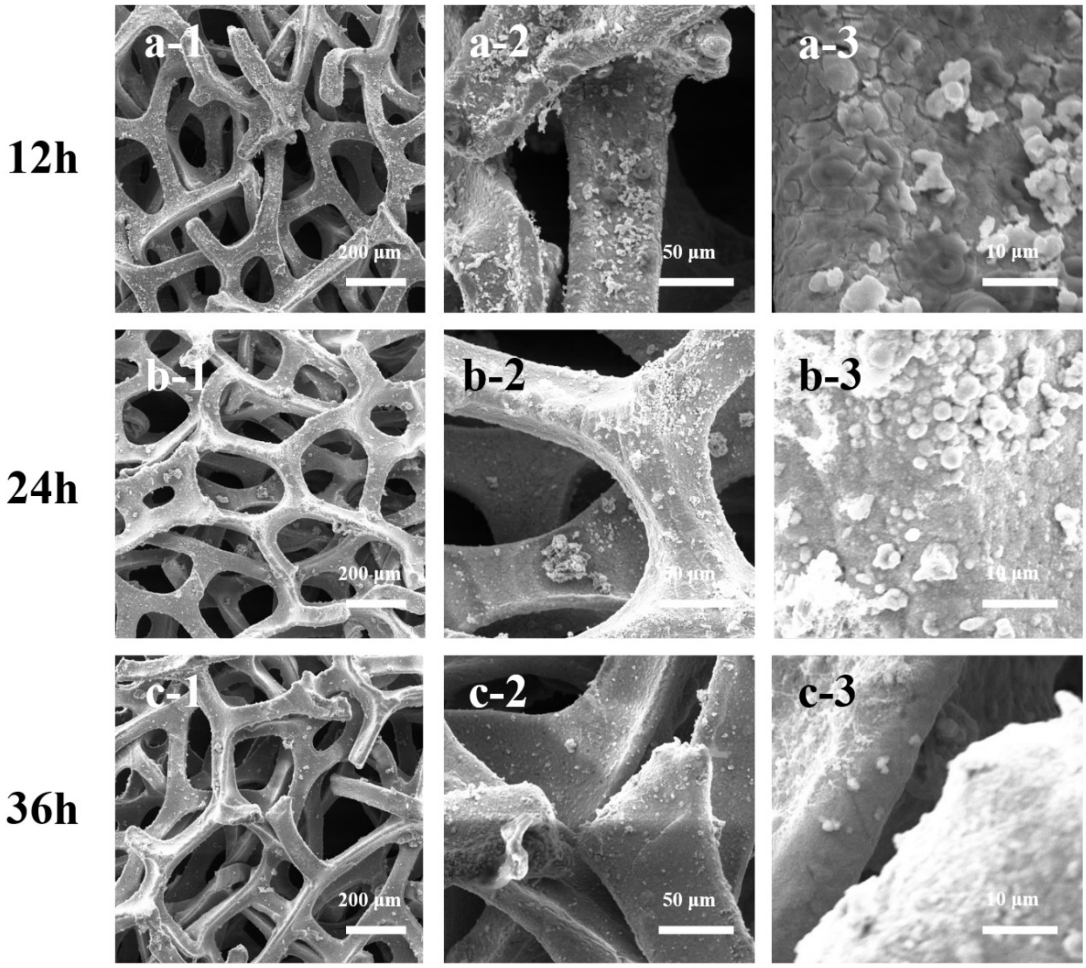

Figure S7 SEM images of Ru@P-NF with different reaction time (12, 24 and 36 h).

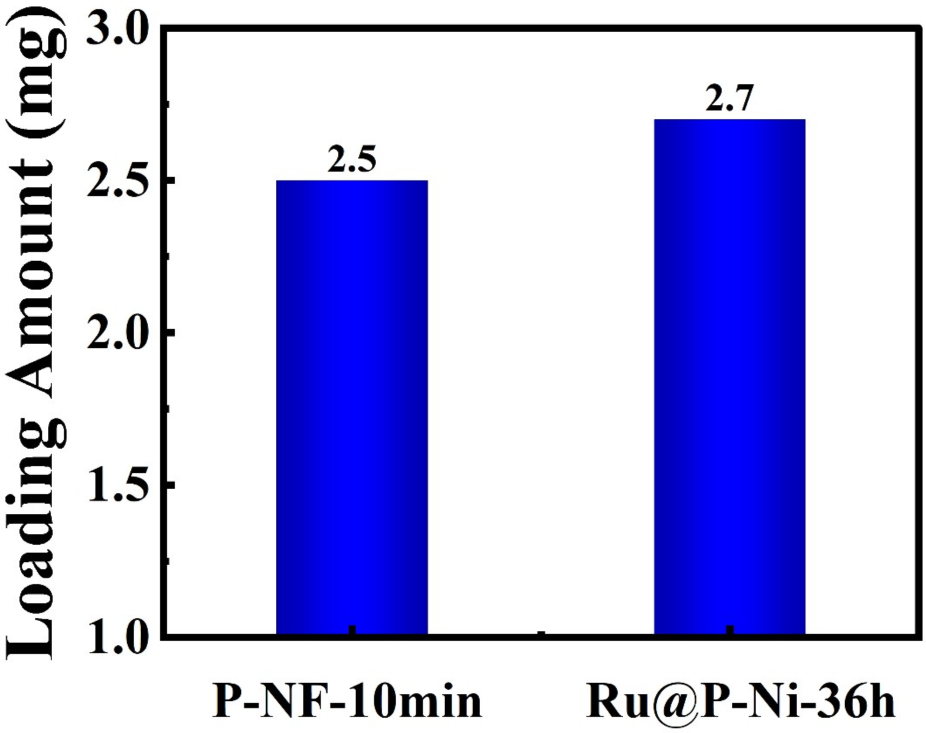

Figure S8 The loading amount of $RuCl_3$ on P-NF at 10 min and 36 h.

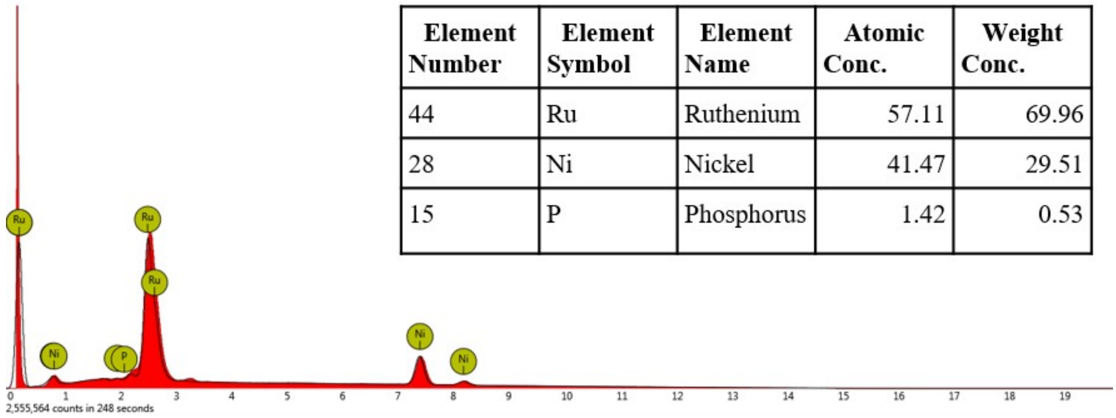

Element Number	Element Symbol	Element Name	Atomic Conc.	Weight Conc.
44	Ru	Ruthenium	57.11	69.96
28	Ni	Nickel	41.47	29.51
15	P	Phosphorus	1.42	0.53

Figure S9 EDS elemental mapping of Ru, Ni and P on the surface.

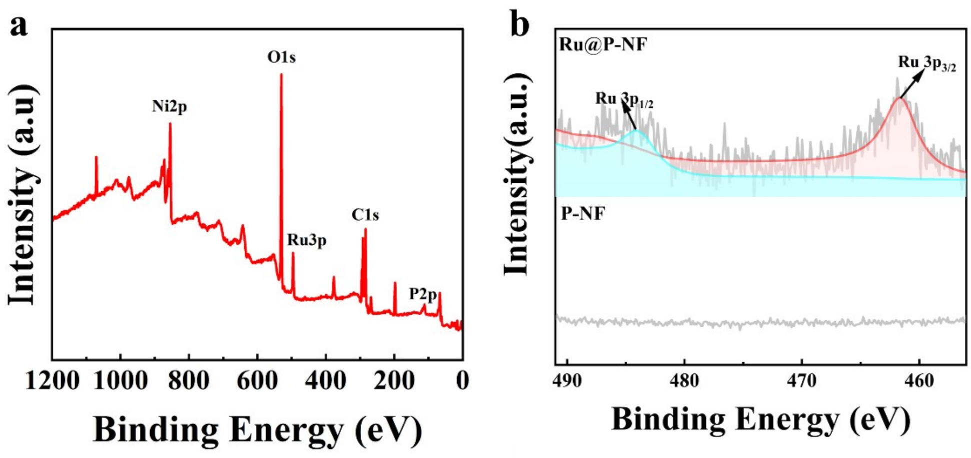

Figure S10 (a) XPS survey spectra of Ru@P-NF. (b) X-ray Photoelectron Spectroscopy for Ru@P-NF and P-NF of Ru 3p orbit.

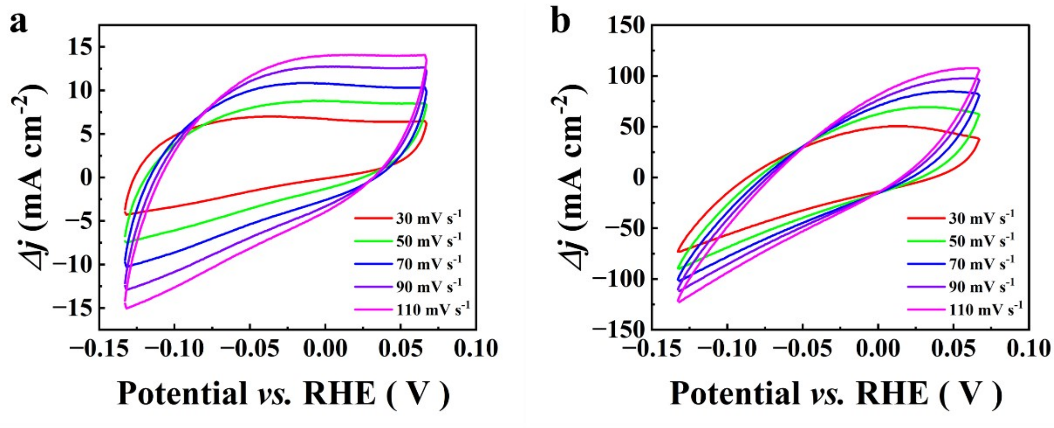

Figure S11 CV curves within a non-faradaic reaction region at different scan rates toward HER process for (a) P-NF and (b) Ru@P-NF electrodes.

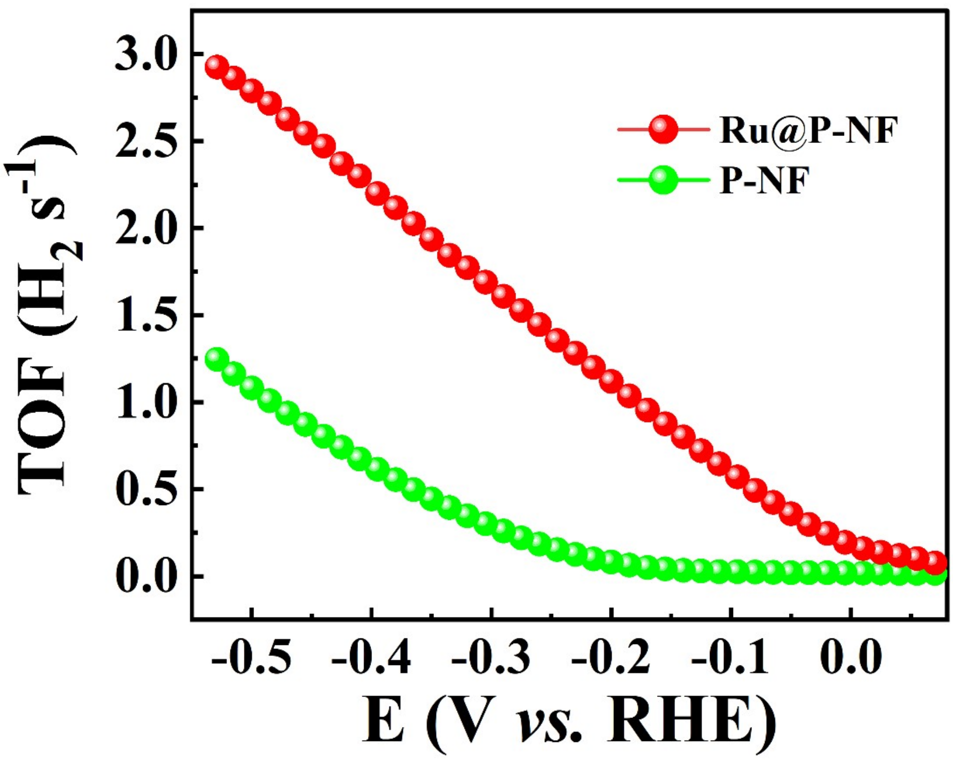

Figure S12 Calculated TOF curves of Ru@P-NF and P-NF electrodes.

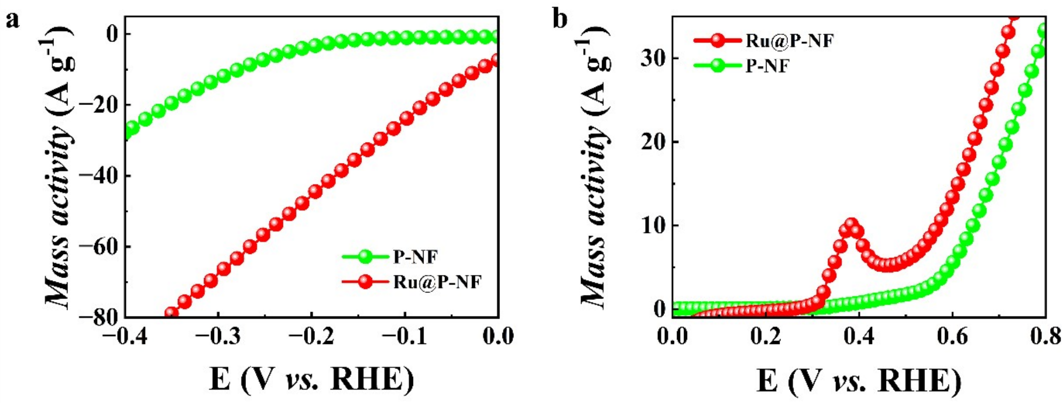

Figure S13 (a) HER Mass-normalization curves. (b) OER Mass-normalization curves.

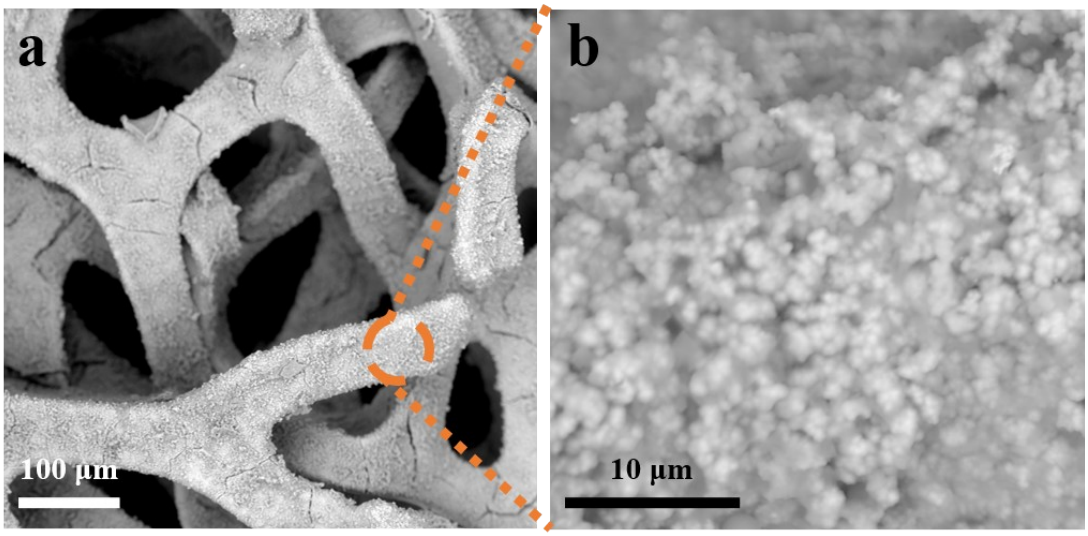

Figure S14 SEM images of post-HER Ru@P-NF electrode.

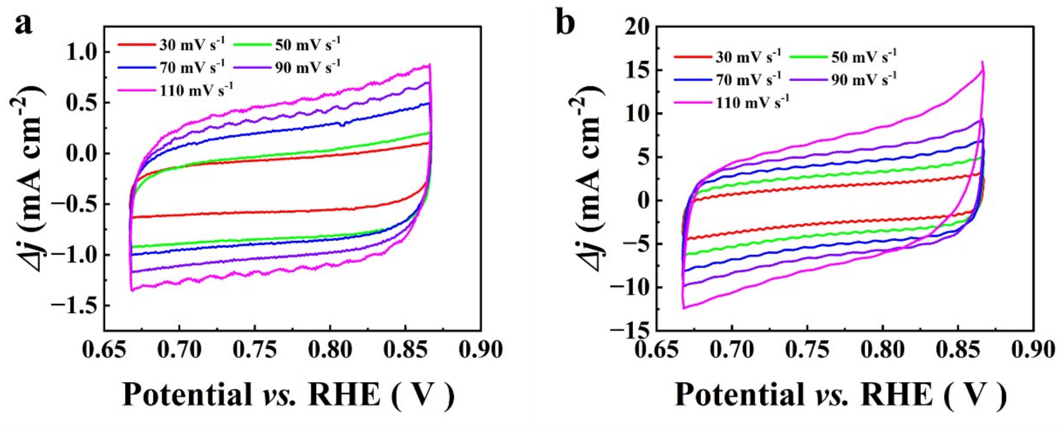

Figure S15 CV curves within a non-faradaic reaction region at different scan rates toward OER process for (a) P-NF and (b) Ru@P-NF electrodes.

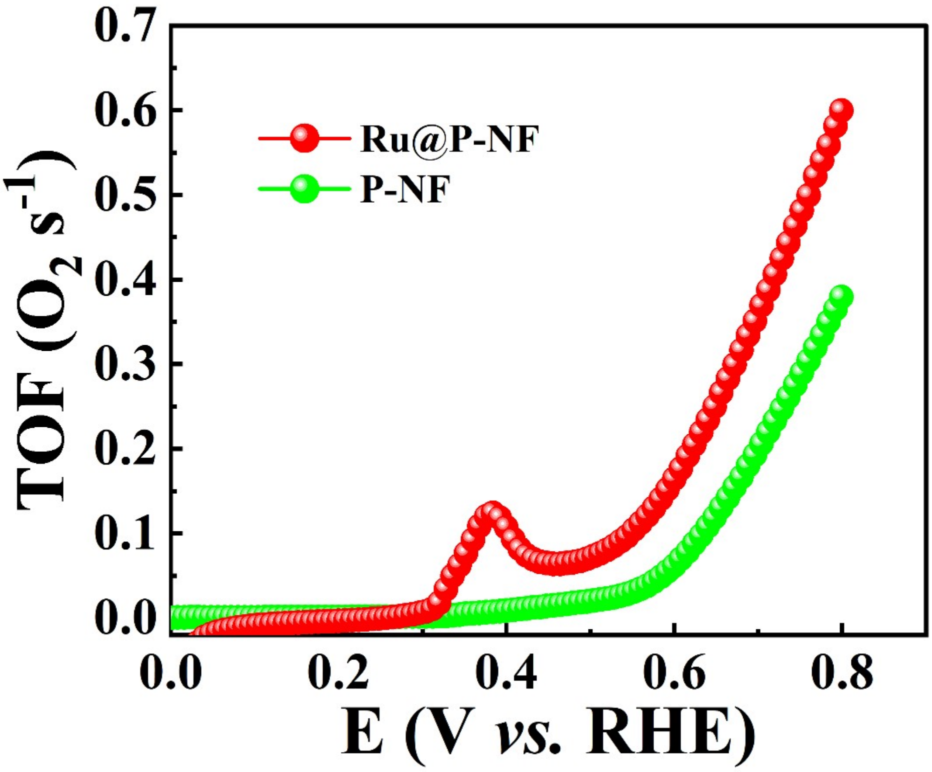

Figure S16 Calculated TOF curves of Ru@P-NF, and P-NF.

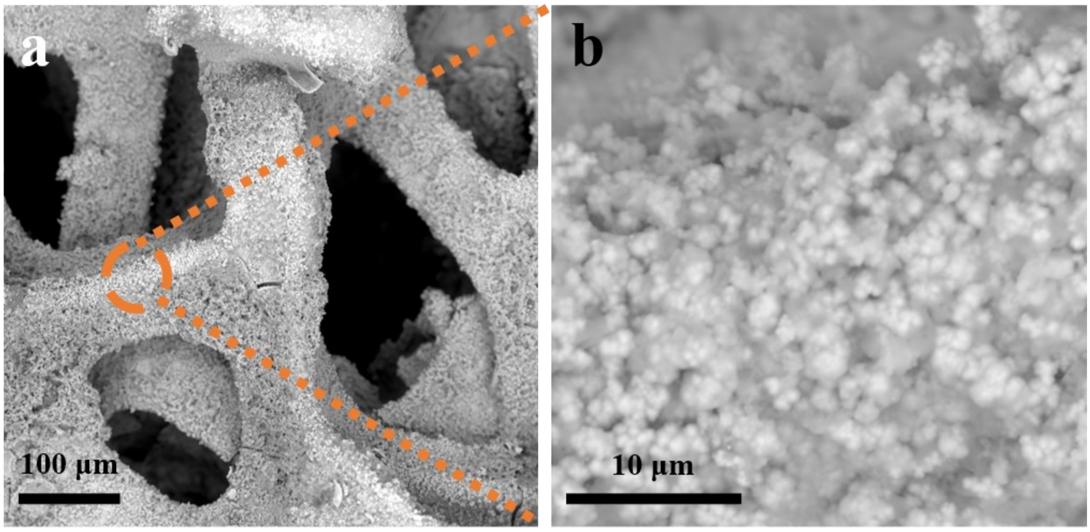

Figure S17 SEM images of post-OER Ru@P-NF electrode.

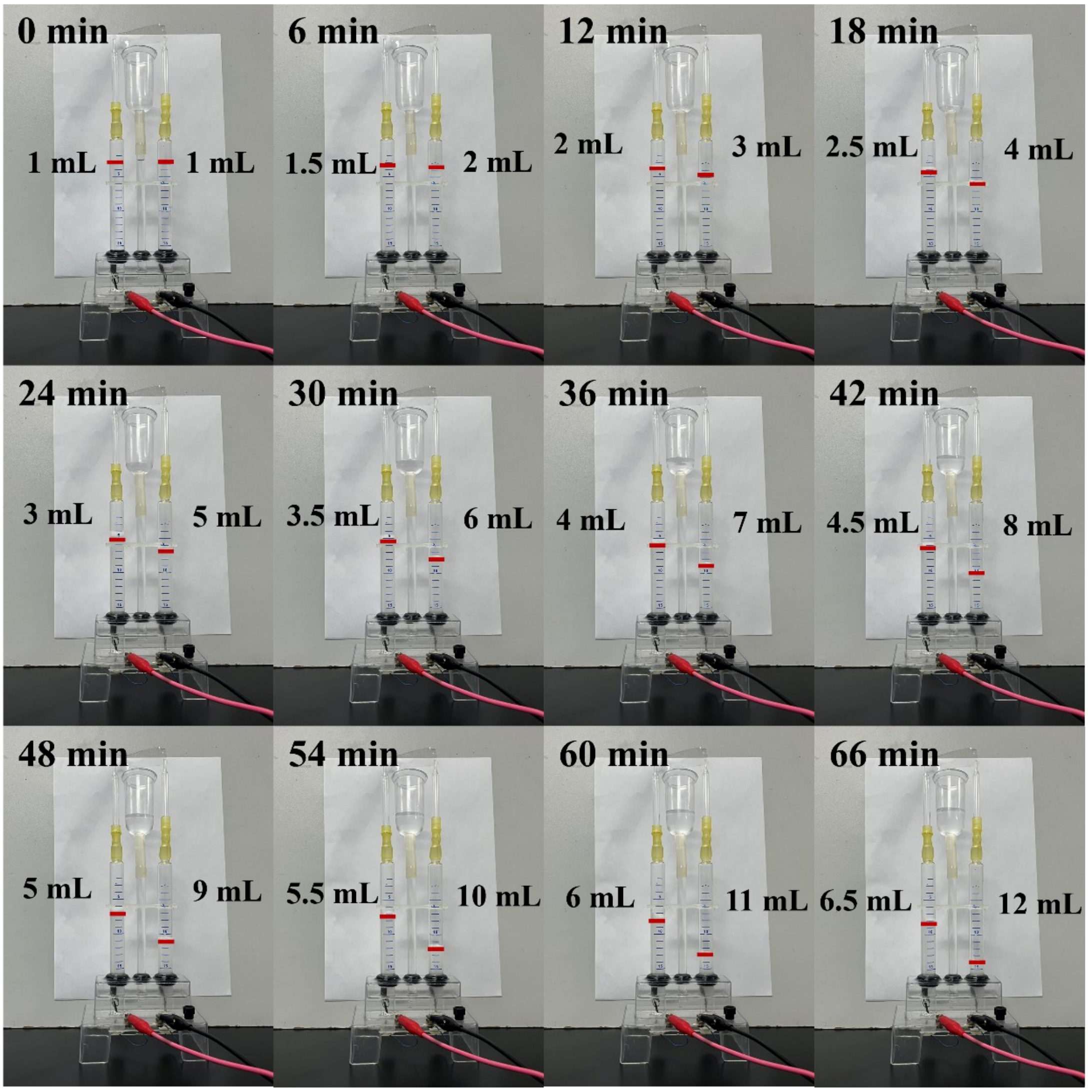

Figure S18 Faradaic efficiency experiment at the current density of 100 mA cm^{-2}.

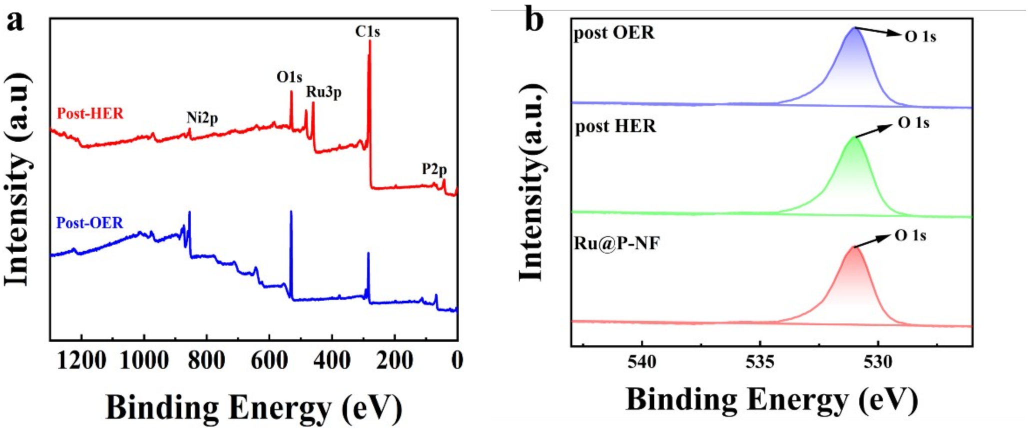

Figure S19 (a) XPS survey spectra of Ru@P-NF. (b) X-ray Photoelectron Spectroscopy for Ru@P-NF and post HER/OER Ni 2p orbit.

Supporting Tables

Table S1. Comparison the HER performance of Ru@P-NF with other electrocatalysts in 1.0 M KOH + 0.5 M NaCl.

Catalyst	**Overpotential**	**Electrolyte**	**References**
Ru@P-NF	η_{100}=32 mV	1.0 M KOH + 0.5 M NaCl	This work
Ru-MnFeP/NF	η_{10}=35 mV	1.0 M KOH + 0.5 M NaCl	[1]
Mo-NiS_x/NF	η_{10}=136 mV	1.0 M KOH + 0.5 M NaCl	[2]
NF/Ni_3S_2/MnS	η_{10}=45 mV	1.0 M KOH + 0.5 M NaCl	[3]
Ru-NiCoP/NF	η_{10}=44 mV	1.0 M KOH + 0.5 M NaCl	[4]
RuIr-NC	η_{10}=46 mV	0.05 M H_2SO_4	[5]
Co-RuIr	η_{10}=14 mV	0.1 M $HClO_4$	[6]
$Ru_{0.5}Ir_{0.5}$	η_{10}=28 mV	1.0 M KOH	[7]
RuCu NSs/C	η_{10}=20 mV	1.0 M KOH	[8]
RuIrTe NTs	η_{10}=29 mV	0.5 M H_2SO_4	[9]
$FexNi_3$-xS_2@NF	η_{10}=72 mV	1.0 M KOH + 0.5 M NaCl	[10]
FeB_2	η_{10}=61 mV	1.0 M KOH + 0.5 M NaCl	[11]
Fe-Ni_2P@C/NF	η_{10}=75 mV	1.0 M KOH + 0.5 M NaCl	[12]
Er-NiCoP/NF	η_{10}=46 mV	1.0 M KOH + 0.5 M NaCl	[13]
$F_{0.25}C_1$CH/NF	η_{10}=77 mV	1.0 M KOH + 0.5 M NaCl	[14]
P-CoFe-LDH@MXene/NF	η_{10}=85 mV	1.0 M KOH + 0.5 M NaCl	[15]
Co-VO_x-P	η_{10}=98 mV	1.0 M KOH + 0.5 M NaCl	[16]

NiCo-LDH	η_{10}=168 mV	1.0 M KOH + 0.5 M NaCl	[17]
Ru-G/CC	η_{10}=40 mV	1.0 M KOH + 0.5 M NaCl	[18]
NiSe@CNTs	η_{10}=27 mV	1.0 M KOH + 0.5 M NaCl	[19]
W_2N/WC	η_{10}=148.5 mV	1.0 M KOH + 0.5 M NaCl	[20]
MoS_2	η_{10}=48 mV	1.0 M KOH + 0.5 M NaCl	[21]
CS-NFO@PNC-700	η_{10}=200 mV	1.0 M KOH + 0.5 M NaCl	[22]
Fe-Ni_5P_4/NiFeOH	η_{10}=197 mV	1.0 M KOH + 0.5 M NaCl	[23]
W-$NiS_{0.5}Se_{0.5}$	η_{10}=39 mV	1.0 M KOH + 0.5 M NaCl	[24]
FeOOH/Ni_3N	η_{10}=67 mV	1.0 M KOH + 0.5 M NaCl	[25]

Table S2. Comparison the OER performance of Ru@P-NF with other electrocatalysts in 1.0 M KOH + 0.5 M NaCl.

Catalyst	**Overpotential**	**Electrolyte**	**References**
Ru@P-NF	η_{10}=153 mV	1.0 M KOH + 0.5 M NaCl	This work
Ru-MnFeP/NF	η_{20}=191 mV	1.0 M KOH + 0.5 M NaCl	[1]
Mo-NiS_x/NF	η_{50}=307 mV	1.0 M KOH + 0.5 M NaCl	[2]
NF/Ni_3S_2/MnS	η_{100}=245 mV	1.0 M KOH + 0.5 M NaCl	[3]
Ru-NiCoP/NF	η_{20}=216 mV	1.0 M KOH + 0.5 M NaCl	[4]
RuIr-NC	η_{10}=165 mV	0.05 M H_2SO_4	[5]
Co-RuIr	η_{10}=235 mV	0.1 M $HClO_4$	[6]
$Ru_{0.5}Ir_{0.5}$	η_{10}=176 mV	1.0 M KOH	[7]
RuCu NSs/C	η_{10}=234 mV	1.0 M KOH	[8]
RuIrTe NTs	η_{10}=205 mV	0.5 M H_2SO_4	[9]
(cannot be measured stably)			
FexNi$_3$-xS$_2$@NF	η_{100}=252 mV	1.0 M KOH + 0.5 M NaCl	[10]
FeB_2	η_{10}=296 mV	1.0 M KOH + 0.5 M NaCl	[11]
Fe-Ni_2P@C/NF	η_{400}=269 mV	1.0 M KOH + 0.5 M NaCl	[12]
Er-NiCoP/NF	η_{10}=225 mV	1.0 M KOH + 0.5 M NaCl	[13]
$F_{0.25}C_1$CH/NF	η_{10}=228 mV	1.0 M KOH + 0.5 M NaCl	[14]
P-CoFe-LDH@MXene/NF	η_{200}=252 mV	1.0 M KOH + 0.5 M NaCl	[15]
Co-VO_x-P	η_{100}=230 mV	1.0 M KOH + 0.5 M NaCl	[16]

NiCo-LDH	η_{30}=278 mV	1.0 M KOH + 0.5 M NaCl	[17]
Ru-G/CC	η_{10}=270 mV	1.0 M KOH + 0.5 M NaCl	[18]
Ni-Fe-Se / NF	η_{100}=222 mV	1.0 M KOH + 0.5 M NaCl	[19]
W_2N/WC	η_{10}=320 mV	1.0 M KOH + 0.5 M NaCl	[20]
MoS_2	η_{10}=260 mV	1.0 M KOH + 0.5 M NaCl	[21]
CS-NFO@PNC-700	η_{10}=217 mV	1.0 M KOH + 0.5 M NaCl	[22]
Fe-Ni_5P_4/NiFeOH	η_{10}=221 mV	1.0 M KOH + 0.5 M NaCl	[23]
W-$NiS_{0.5}Se_{0.5}$	η_{10}=171 mV	1.0 M KOH + 0.5 M NaCl	[24]
FeOOH/Ni_3N	η_{10}=224 mV	1.0 M KOH + 0.5 M NaCl	[25]

Table S3. The overall-water splitting performance for Ru@P-NF electrode and other electrodes with non-noble-metal electrocatalysts in 1.0 M KOH + 0.5 M NaCl.

Catalyst	Overpotential	Electrolyte	References
Ru@P-NF	η_{20}=1.42 V	1.0 M KOH + 0.5 M NaCl	This work
Ru-MnFeP/NF	η_{10}=1.47 V	1.0 M KOH + 0.5 M NaCl	[1]
Mo-NiS_x/NF	η_{10}=1.594 V	1.0 M KOH + 0.5 M NaCl	[2]
NF/Ni_3S_2/MnS	η_{20}=1.53 V	1.0 M KOH + 0.5 M NaCl	[3]
Ru-NiCoP/NF	η_{10}=1.515 V	1.0 M KOH + 0.5 M NaCl	[4]
RuIr-NC	η_{10}=1.485 V	0.05 M H_2SO_4	[5]
Co-RuIr	η_{10}=1.52 V	0.1 M $HClO_4$	[6]
$Ru_{0.5}Ir_{0.5}$	η_{10}=1.48 V	1.0 M KOH	[7]
RuCu NSs/C	η_{10}=1.49 V	1.0 M KOH	[8]
RuIrTe NTs	η_{10}=1.511 V	0.5 M H_2SO_4	[9]
$FexNi_3$-xS_2@NF	η_{10}=1.51 V	1.0 M KOH + 0.5 M NaCl	[10]
FeB_2	η_{10}=1.57 V	1.0 M KOH + 0.5 M NaCl	[11]
Fe-Ni_2P@C/NF	η_{100}=1.55 V	1.0 M KOH + 0.5 M NaCl	[12]
FeP_x/Fe–N–C/NPC	η_{10}=1.58 V	1.0 M KOH + 0.5 M NaCl	[26]
$F_{0.25}C_1$CH/NF	η_{10}=1.45 V	1.0 M KOH + 0.5 M NaCl	[14]
P-CoFe-LDH@MXene/NF	η_{10}=1.52 V	1.0 M KOH + 0.5 M NaCl	[15]
Fe-doped CoP nanoarray	η_{10}=1.6 V	1.0 M KOH + 0.5 M NaCl	[27]
NiCo-LDH	η_{10}=1.63 V	1.0 M KOH + 0.5 M NaCl	[17]

Ni-MoO2/NF-IH and NiFe LDH/NF-IH	η_{10}=1.5 V	1.0 M KOH + 0.5 M NaCl	[28]
NiSe@CNTs	η_{500}=1.72 V	1.0 M KOH + 0.5 M NaCl	[13]
Ni_3N-NiMoN catalysts	η_{10}=1.54 V	1.0 M KOH + 0.5 M NaCl	[29]
MoS_2	η_{10}=1.45 V	1.0 M KOH + 0.5 M NaCl	[21]
CS-NFO@PNC-700	η_{500}=1.861 V	1.0 M KOH + 0.5 M NaCl	[22]
Fe-Ni_5P_4/NiFeOH	η_{10}=1.55 V	1.0 M KOH + 0.5 M NaCl	[23]
Co_4S_3/Mo_2C-NSC	η_{10}=1.62 V	1.0 M KOH + 0.5 M NaCl	[30]
FeOOH/Ni_3N	η_{10}=1.56 V	1.0 M KOH + 0.5 M NaCl	[25]

References

1 D. Chen, Z. Pu, R. Lu, P. Ji, P. Wang, J. Zhu, C. Lin, H. Li, X. Zhou, Z. Hu, F. Xia, J. Wu, S. Mu. Ultralow Ru Loading Transition Metal Phosphides as High-Efficient Bifunctional Electrocatalyst for a Solar-to-Hydrogen Generation System[J]. Advanced Energy Materials, 2020, 10(28): 2000814.

2 Y. Zhang, M. Chen, P. Guo, Y. Du, B. Song, X. Wang, Z. Jiang, P. Xu. *Retracted* : Magnetic field-enhanced water splitting enabled by bifunctional molybdenum-doped nickel sulfide on nickel foam[J]. Carbon Energy, 2023: e351.

3 Y. Zhang, J. Fu, H. Zhao, R. Jiang, F. Tian, R. Zhang. Tremella-like Ni3S2/MnS with ultrathin nanosheets and abundant oxygen vacancies directly used for high speed overall water splitting[J]. Applied Catalysis B: Environmental, 2019, 257: 117899.

4 D. Chen, R. Lu, Z. Pu, J. Zhu, H.-W. Li, F. Liu, S. Hu, X. Luo, J. Wu, Y. Zhao, S. Mu. Ru-doped 3D flower-like bimetallic phosphide with a climbing effect on overall water splitting[J]. Applied Catalysis B: Environmental, 2020, 279: 119396.

5 D. Wu, K. Kusada, S. Yoshioka, T. Yamamoto, T. Toriyama, S. Matsumura, Y. Chen, O. Seo, J. Kim, C. Song, S. Hiroi, O. Sakata, T. Ina, S. Kawaguchi, Y. Kubota, H. Kobayashi, H. Kitagawa. Efficient overall water splitting in acid with anisotropic metal nanosheets[J]. Nature Communications, 2021, 12(1): 1145.

6 J. Shan, T. Ling, K. Davey, Y. Zheng, S. Qiao. Transition-Metal-Doped RuIr Bifunctional Nanocrystals for Overall Water Splitting in Acidic Environments[J]. Advanced Materials, 2019, 31(17): 1900510.

7 Y. Jiang, Y. Mao, Y. Jiang, H. Liu, W. Shen, M. Li, R. He. Atomic equidistribution enhanced RuIr electrocatalysts for overall water splitting in the whole pH range[J]. Chemical Engineering Journal, 2022, 450: 137909.

8 Q. Yao, B. Huang, N. Zhang, M. Sun, Q. Shao, X. Huang. Channel-Rich RuCu Nanosheets for pH-Universal Overall Water Splitting Electrocatalysis[J]. Angewandte Chemie, 2019, 131(39): 14121–14126.

9 M. Liu, S. Liu, Q. Mao, S. Yin, Z. Wang, Y. Xu, X. Li, L. Wang, H. Wang. Ultrafine ruthenium–iridium–tellurium nanotubes for boosting overall water splitting in acidic media[J]. Journal of Materials Chemistry A, 2022, 10(4): 2021–2026.

10 B. Fei, Z. Chen, J. Liu, H. Xu, X. Yan, H. Qing, M. Chen, R. Wu. Ultrathinning Nickel Sulfide with Modulated Electron Density for Efficient Water Splitting[J]. Advanced Energy Materials, 2020, 10(41): 2001963.

11 H. Li, P. Wen, Q. Li, C. Dun, J. Xing, C. Lu, S. Adhikari, L. Jiang, D. L. Carroll, S. M. Geyer. Retracted: Earth-Abundant Iron Diboride (FeB_2) Nanoparticles as Highly Active Bifunctional Electrocatalysts for Overall Water Splitting[J]. Advanced Energy Materials, 2017, 7(17): 1700513.

12 D. Li, Z. Li, R. Zou, G. Shi, Y. Huang, W. Yang, W. Yang, C. Liu, X. Peng. Coupling overall water splitting and biomass oxidation via Fe-doped Ni2P@C nanosheets at large current density[J]. Applied Catalysis B: Environmental, 2022, 307: 121170.

13 H. Zhang, A. Aierke, Y. Zhou, Z. Ni, L. Feng, A. Chen, T. Wågberg, G. Hu. A

high-performance transition-metal phosphide electrocatalyst for converting solar energy into hydrogen at 19.6% STH efficiency[J]. Carbon Energy, 2023, 5(1): e217.

14 L. Hui, Y. Xue, D. Jia, H. Yu, C. Zhang, Y. Li. Multifunctional Single-Crystallized Carbonate Hydroxides as Highly Efficient Electrocatalyst for Full Water splitting[J]. Advanced Energy Materials, 2018, 8(20): 1800175.
15 L. Deng, K. Zhang, D. Shi, S. Liu, D. Xu, Y. Shao, J. Shen, Y. Wu, X. Hao. Rational design of Schottky heterojunction with modulating surface electron density for high-performance overall water splitting[J]. Applied Catalysis B: Environmental, 2021, 299: 120660.
16 Z. Zhu, K. Xu, W. Guo, H. Zhang, X. Xiao, M. He, T. Yu, H. Zhao, D. Zhang, T. Yang. Vanadium-phosphorus incorporation induced interfacial modification on cobalt catalyst and its super electrocatalysis for water splitting in alkaline media[J]. Applied Catalysis B: Environmental, 2022, 304: 120985.
17 J. Yan, L. Chen, X. Liang. Co9S8 nanowires@NiCo LDH nanosheets arrays on nickel foams towards efficient overall water splitting[J]. Science Bulletin, 2019, 64(3): 158–165.
18 M. You, X. Du, X. Hou, Z. Wang, Y. Zhou, H. Ji, L. Zhang, Z. Zhang, S. Yi, D. Chen. In-situ growth of ruthenium-based nanostructure on carbon cloth for superior electrocatalytic activity towards HER and OER[J]. Applied Catalysis B: Environmental, 2022, 317: 121729.
19 H. Xue, T. Yang, Z. Zhang, Y. Zhang, Z. Geng, Y. He. Stimulate the hidden catalysis potential and exposure of nickel site in NiSe@CNTs result in ultra-high HER/OER activity and stability[J]. Applied Catalysis B: Environmental, 2023, 330: 122641.
20 J. Diao, Y. Qiu, S. Liu, W. Wang, K. Chen, H. Li, W. Yuan, Y. Qu, X. Guo. Interfacial Engineering of W_2N/WC Heterostructures Derived from Solid-State Synthesis: A Highly Efficient Trifunctional Electrocatalyst for ORR, OER, and HER[J]. Advanced Materials, 2020, 32(7): 1905679.
21 Q. Xiong, Y. Wang, P. Liu, L. Zheng, G. Wang, H. Yang, P. Wong, H. Zhang, H. Zhao. Cobalt Covalent Doping in MoS_2 to Induce Bifunctionality of Overall Water Splitting[J]. Advanced Materials, 2018, 30(29): 1801450.
22 S. Ramakrishnan, D. B. Velusamy, S. Sengodan, G. Nagaraju, D. H. Kim, A. R. Kim, D. J. Yoo. Rational design of multifunctional electrocatalyst: An approach towards efficient overall water splitting and rechargeable flexible solid-state zinc–air battery[J]. Applied Catalysis B: Environmental, 2022, 300: 120752.
23 C.-F. Li, J.-W. Zhao, L.-J. Xie, J.-Q. Wu, G.-R. Li. Fe doping and oxygen vacancy modulated Fe-Ni5P4/NiFeOH nanosheets as bifunctional electrocatalysts for efficient overall water splitting[J]. Applied Catalysis B: Environmental, 2021, 291: 119987.
24 Y. Wang, X. Li, M. Zhang, J. Zhang, Z. Chen, X. Zheng, Z. Tian, N. Zhao, X. Han, K. Zaghib, Y. Wang, Y. Deng, W. Hu. Highly Active and Durable Single-Atom Tungsten-Doped $NiS_{0.5}Se_{0.5}$ Nanosheet @ $NiS_{0.5}Se_{0.5}$ Nanorod Heterostructures for Water Splitting[J]. Advanced Materials, 2022, 34(13): 2107053.

25 J. Guan, C. Li, J. Zhao, Y. Yang, W. Zhou, Y. Wang, G.-R. Li. FeOOH-enhanced bifunctionality in Ni3N nanotube arrays for water splitting[J]. Applied Catalysis B: Environmental, 2020, 269: 118600.
26 Q. Qin, H. Jang, P. Li, B. Yuan, X. Liu, J. Cho. A Tannic Acid–Derived N-, P-Codoped Carbon-Supported Iron-Based Nanocomposite as an Advanced Trifunctional Electrocatalyst for the Overall Water Splitting Cells and Zinc–Air Batteries[J]. Advanced Energy Materials, 2019, 9(5): 1803312.
27 C. Tang, R. Zhang, W. Lu, L. He, X. Jiang, A. M. Asiri, X. Sun. Fe-Doped CoP Nanoarray: A Monolithic Multifunctional Catalyst for Highly Efficient Hydrogen Generation[J]. Advanced Materials, 2017, 29(2): 1602441.
28 G. Xiong, Y. Chen, Z. Zhou, F. Liu, X. Liu, L. Yang, Q. Liu, Y. Sang, H. Liu, X. Zhang, J. Jia, W. Zhou. Rapid Synthesis of Various Electrocatalysts on Ni Foam Using a Universal and Facile Induction Heating Method for Efficient Water Splitting[J]. Advanced Functional Materials, 2021, 31(15): 2009580.
29 A. Wu, Y. Xie, H. Ma, C. Tian, Y. Gu, H. Yan, X. Zhang, G. Yang, H. Fu. Integrating the active OER and HER components as the heterostructures for the efficient overall water splitting[J]. Nano Energy, 2018, 44: 353–363.
30 Y. Liu, X. Luo, C. Zhou, S. Du, D. Zhen, B. Chen, J. Li, Q. Wu, Y. Iru, D. Chen. A modulated electronic state strategy designed to integrate active HER and OER components as hybrid heterostructures for efficient overall water splitting[J]. Applied Catalysis B: Environmental, 2020, 260: 118197.